Seismic Imaging with Application to Mine Layout and Development

Greenhalgh, S.[1], and Mason, I.[2]

1. School of Earth Sciences, Flinders University, Adelaide, South Australia, Australia
2. Dept. of Geology and Geophysics, University of Sydney, New South Wales, Australia

ABSTRACT

Significant progress has been made towards the goal of generating detailed seismic images as an aid to mining and exploration at Kambalda, Western Australia. Crosshole instrumentation including a slimline multi-element hydrophone array and a downhole electric discharge sparker sound source, have been developed.

Seismic trials at a number of mines have established that high frequency signals can be propagated over distances in excess of 100 metres. Tomographic as well as 3-D reflection imaging techniques have been applied to the data to produce useful pictures of the ore and host rock. Ultrasonic measurements made on core samples are helpful in tomogram interpretation, but interpretation remains ambiguous. Combined seismic and radar experiments are needed to properly delineate mineralisation.

INTRODUCTION

The costs of exploration for nickel sulphide ore bodies in the Kambalda area of Western Australia have risen significantly by the need to drill to depths of over 600 m before encountering prospective horizons. It is impossible at such depths to spatially sample the ore-bearing contact zone with anything like the sampling density required to detect and delineate an ore body. Underground drilling experience suggests that it is necessary to core on a 20×20 m grid in order to be certain of not missing any economically relevant ore bodies on the Lunnon Basalt–Ultramafic contact zone. The core from any borehole that just misses an ore body carries very little evidence of the body's presence. The cores that are taken from an ore body give little indication of its size. Most ore bodies are tubular in shape, less than two metres in thicknesses, and broken up into surfaces often less than 20 m long.

The odds of striking ore while drilling blind would improve if we had the technology to support a 'homing torpedo' type of drill bit. The seismic method provides one such technology. Ground penetrating radar (GPR), applied potential (resistivity imaging), and radio wave imaging (RIM), are others.

These latter three methods all depend on there being sufficient electrical contrast between mineralisation and the host rock. Radar is being used with considerable effect at Kambalda to detect and outline ore bodies underground within the mine by running borehole profiles and scans (Turner, pers. comm.). However, given the limited penetration of 50 MHz radar signals (<50 m) even in favourably resistive rock, GPR cannot be used in exploration from the surface because of the large hole separation (>200 m) and the presence of saline water and other conductors (e.g., salt lakes).

Applied potential (AP) measurements have been conducted only sparingly at Kambalda to determine continuity of ore (conductors) between drillhole intersections. A research programme to extend AP to cross-hole resistivity imaging at Kambalda, involving numerous current injection points and borehole potential measurements, is about to start.

A new RIM tool is being built at Sydney University by one of us (IMM). It offers considerable scope for ore delineation but to date no such radio wave surveys have been undertaken in any of the Kambalda mines. We are aware that encouraging RIM results have been obtained in coal mines in Australia and the U.S., and for base metal exploration at Broken Hill and Mount Isa, Australia. RIM is expected to offer improved penetration (hundreds of metres) but less resolution than GPR.

There are potentially great economic benefits to be obtained from an ability to seismically probe ahead of a mine face, or to image with a reasonable clarity a volume of rock surrounding an exploration or development borehole. The sort of geological information that a high frequency (200–2000 Hz) seismic technique can, in principle, provide includes:

- existence of ore,
- changes of rock type,
- offset of mineralisation,
- location of structure (faults, troughs, etc.),
- extent of shear zones.

In "Proceedings of Exploration 97: Fourth Decennial International Conference on Mineral Exploration" *edited by* A.G. Gubins, 1997, p. 585–598

The seismic technique offers good resolving power (a few metres) coupled with a sufficient degree of penetration (probing distance tens to hundreds of metres). However, ore bodies and associated structures present elusive seismic targets. To date, relatively few successful hard rock seismic surveys have been carried out in metalliferous mining areas. Surface reflection surveys for mapping mineralisation have been reported by Singh (1983), Nelson (1984), Gal'perin (1984), Dahle *et al.* (1985), Campbell and Crotty (1988), Spencer *et al.* (1993), Wright *et al.* (1994) and Adam *et al.* (1996). Underground reflection and transmission measurements in hard rock mines, and crosshole exploration surveys in crystalline rock, have been carried out in Germany (Schmidt, 1959; Wachsmuth and Schmidt, 1962), Southern Africa (Reid *et al.*, 1979; Mutyorauta, 1987; Carneiro and Gendzwill, 1996), USA (Gupta, 1971; Price, 1974; Ruskey, 1981; Peterson, 1985; Freidel *et al.*, 1995), Canada (Wong *et al.*, 1984; Young *et al.*, 1989; Gendzeill and Brehm, 1993), Sweden (Gustavson *et al.*, 1984), Finland (Cosma, 1983) and Australia (Harman *et al.*, 1987; Duncan *et al.*, 1989; Sinadinovski *et al.*, 1995).

In 1992 a major research programme was initiated by Western Mining Corp. at Kambalda to develop high resolution seismic and radar imaging techniques to aid mining of and exploration for nickel sulphide ore bodies. The economic justification is improved cost effectiveness (and safety) of underground development, ore body delineation and surface exploration. This paper provides a summary on some of the seismic work done and imaging results obtained at just one mine site with both the seismic tomography and seismic reflection techniques.

THE KAMBALDA NICKEL SULPHIDE ENVIRONMENT

The Kambalda region is situated within the south central part of the Norseman-Wiluna greenstone belt, in the Eastern Goldfields Province of the Archaean Yilgarn Craton. The town of Kambalda is located 560 km east of Perth.

The volcanic-sedimentary sequence at Kambalda, with its enclosed magmatic nickel sulphide deposits, has undergone deformation, metamorphism, intrusive activity and late stage gold mineralisation. (Cowden and Roberts, 1990).

Many rocks in this region have undergone upper greenschist to lower amphibolite-facies metamorphism. Serpentinisation and talc-carbonate alteration occurred with prograde metamorphism. There has also been a series of intrusions of mafic to felsic stocks, dykes and sills and granitoid bodies.

The ribbon-like nickel sulphide bodies occur at the base of the lowermost lava flows of a komatiite pile in the contact ore position immediately overlying basalt, or at the base of the next one or two flows in the hanging wall position The sulphide bodies are typically stratified with sulphide content decreasing upwards. A lowermost massive ore (>80%) pyrrhotite-pentlandite layer is overlain by a matrix (40 to 80%) and disseminated (<40%) sulphide layers. There are significant differences in mineralogy between the massive, matrix and disseminated layers and in nickel content (tenor) between different ore bodies.

The morphology of the ore zone is highly variable with the massive sulphide layers being irregular in thickness (generally less than 5 m). The matrix and disseminated layers are more regular in distribution and generally comprise 60 to 80% of the total thickness of the sulphide zone.

VELOCITIES AND DENSITIES OF ORES AND HOST ROCKS

Over 230 rock core samples from Kambalda were carefully selected and subjected to ultrasonic velocity examination in the laboratory. Densities were also measured. The goal was to elicit the elastic properties of the ore-bearing rocks to establish a physical basis (velocity and/or impedance contrast) for seismic investigations.

The cylindrical core samples (of diameter 51 mm and 35 mm) were cut to roughly 10 cm lengths and the ends squared to accommodate the piezoelectric transducers. The specimens covered a wide range of rocks, including ultramafic, mafic sedimentary, felsic, intermediate and nickel sulphide ore (massive matrix disseminated). Most measurements were made at atmospheric pressure, although 12 samples were analysed under a uniaxial load of 12 kN (corresponding to burial depths of a few hundred metres). The velocities measured under pressure were only 1% to 2% higher than the measurements carried out at atmospheric pressure. We concluded that the pressure effect was minor and could be safely ignored for our purposes.

Table I summarises the longitudinal velocities and densities, giving range as well as mean values. There is considerable overlap in velocity between the various rock types so it is not possible to unambiguously identify the rock on the basis of P-wave velocity alone. The variability within each rock type is due to differences in mineralogy, rock fabric/texture, and rock alteration. Figure 1 shows velocity variation with density for the nickel sulphide ore samples. A definite inverse correlation exists. Density is directly related to ore grade, which is shown in units of $ symbols in Figure 1. High density massive ore is characterised by low velocity.

The laboratory sonic velocities were determined at a frequency of 500 kHz, and proved to be about 20% lower than those measured underground at the Foster mine in a cross-gallery experiment (Fullager *et al.*

Table 1: ***Longitudinal wave velocities and densities of ore and rock samples from Kambalda, Western Australia.***

		Longitudinal Velocity (m/s)		
Rock type	**Number of samples**	**Range**	**Mean ± std. dev.**	**Density Mean ± Std. Dev (g/cm^3)**
Massive ore	9	4190–5750	4880 ± 450	4.30 ± 0.46
Matrix ore	8	4700–6050	5160 ± 440	3.52 ± 0.29
Disseminated ore	45	4140–6610	5440 ± 570	3.06 ± 0.23
Mafic	65	3890–7000 (main cluster 6000–6500)	6050 ± 730	2.93 ± 0.12
Ultramafic	68	2870–7000 (main cluster 5000–6500)	5540 ± 640	2.87 ± 0.09
Felsic [1]	5	3690–5050	4560 ± 530	2.70 ± .01
Intermediate [1]	4	5270–6290	5880 ± 340	2.82 ± 0.05
Sedimentary [1]	5	5170–6200	5770 ± 340	2.75 ± 0.06

1. Insufficient samples

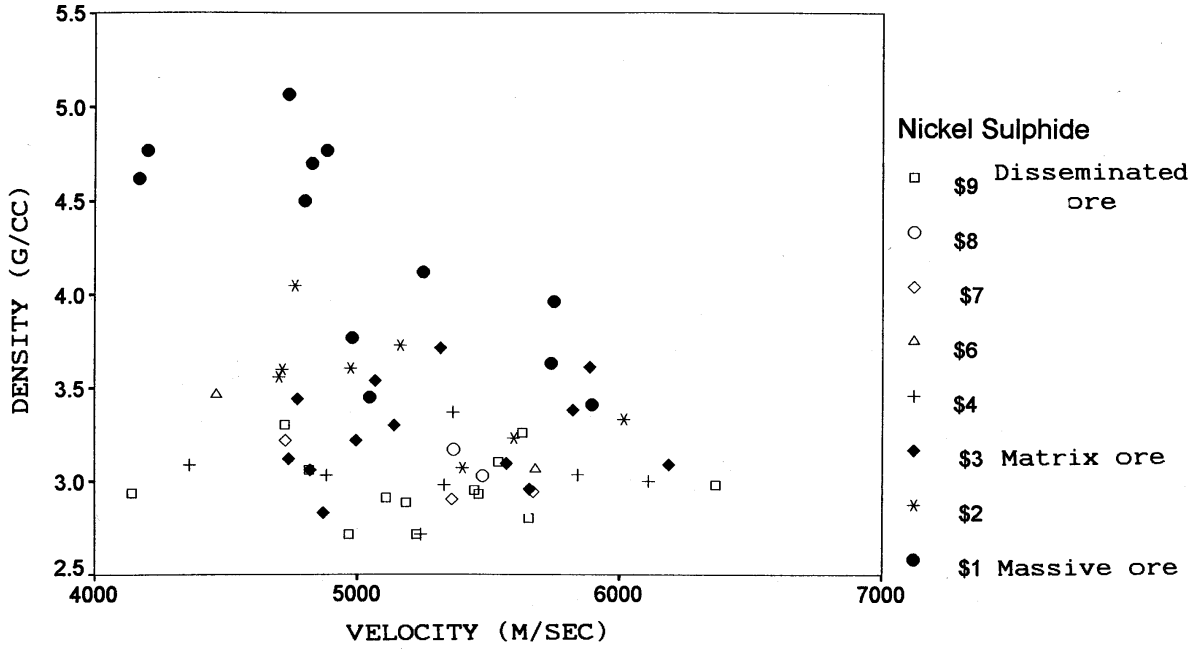

Figure 1: *P-wave velocity versus density for nickel sulphide ore samples.*

1992). Compressional (P) and shear (S) waves from small explosions and hammer blows were observed on a geophone spread over distances of ten to hundreds of metres. Frequencies were 1–3 kHz and velocity of basalt very fast: 6.7 km/s for P wave and 4.0 km/s for S waves.

The normal incidence reflection coefficients for the various rock and ore contacts are listed in Table 2; they are based on the average velocity and densities given in Table I. Boundaries are considered to be detectable by reflection means if the reflection coefficient exceeds 0.03. Thus it appears that there is sufficient density contrast between the ore and the host rock, and sufficient velocity contrast between the basalt and the ultramafics for the seismic method to work at Kambalda. But we still face a formidable set of unknowns. Impedance variations can only be mapped, and the maps interpreted, *if* the target field is sparsely populated; *if* seismic waves can be coupled cleanly into and out of the host continuum; *if* mode conversions and multiple scattering are limited; *if* surface wave noise is not too severe; and *if* the site access is sufficient to sample the wave fields after they have interacted with the target. Most of these questions can only be answered by field trials.

Table 2: ***Reflection coefficients for various rock and ore contacts.***

Contact	R
Ultramafic/Mafic	0.05
Mafic/Massive ore	0.08
Ultramafic/Massive ore	0.15
Mafic/Matrix ore	0.01
Ultramafic/Matrix ore	0.08
Mafic/Disseminated ore	0.03
Ultramafic/Disseminated ore	0.03

SEISMIC MODELLING

Tomography

Figure 2 shows a simplified model, containing a faulted ore body sitting between two horizontal underground boreholes 60 m apart. The ore has low velocity compared to the rock. A set of 24 shots and 24 geophones are placed in the boreholes to simulate a seismic tomography experiment. Shot and detector spacing is 5 m. Raypaths are shown for first arrivals. The synthetic arrival times were then inverted by a DMLS tomography algorithm (Zhou *et al.*, 1992) to produce the tomogram of Figure 3. The ore zones have been recovered albeit with some blurring and distortion due to the limited angular coverage. This model clearly demonstrates the possibilities of tomography in crosswell exploration.

Reflection

To assess the likelihood of detecting reflections from the basalt-ultramafic contact (which contains mineralised portions), a 2-D synthetic shot gather has been computed using a full elastic heterogeneous finite difference code (Cao and Greenhalgh, 1992). The shot receiver geometry replicated that from a typical underground experiment such as that performed at Foster (Fullager *et al.*, 1992). A combined P&S wave source was placed 1.5 m from the decline wall (to simulate an explosive in a shallow shot hole), and a 2-component receiver array of eight sta-

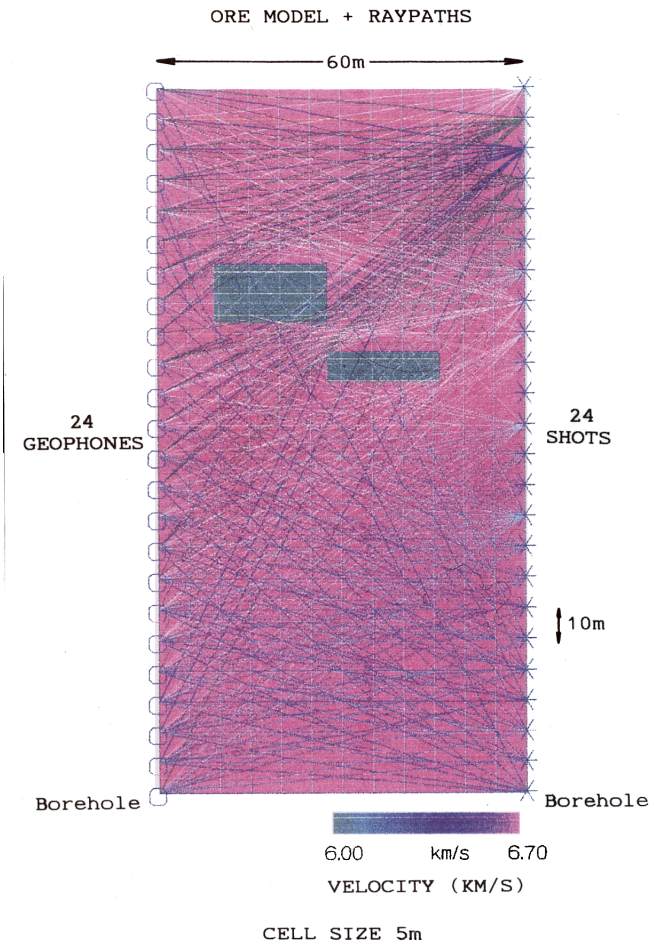

Figure 2: *Synthetic 2-D crosshole seismic experiment showing ore body model and raypaths.*

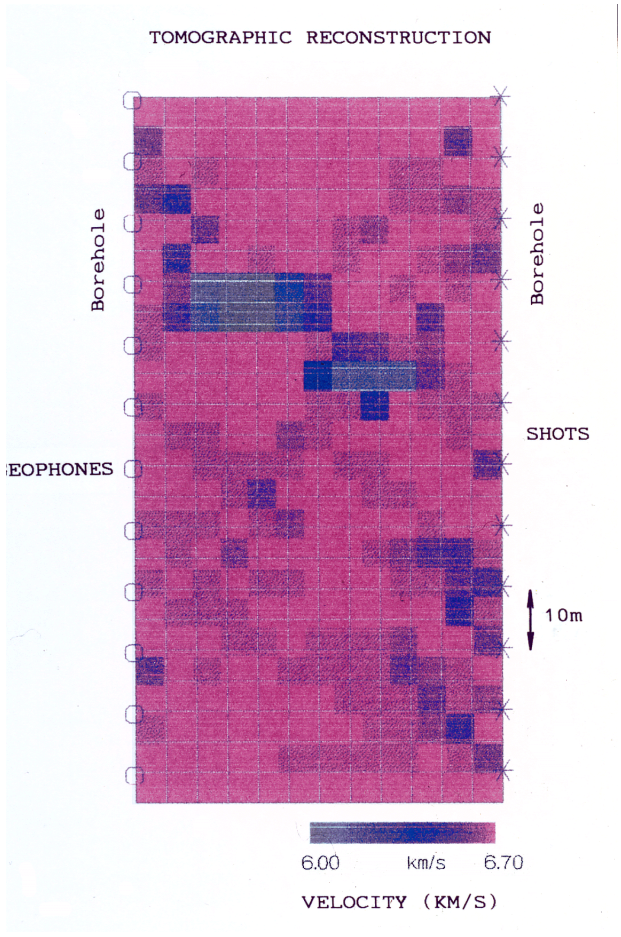

Figure 3: *Velocity tomogram reconstructed for the ore body model of Figure 2.*

tions, spaced 2.5 m apart, was located at a minimum distance of 60 m from the source. The perpendicular distance from the shot-geophone line to the reflector was set at 50 m. A dominant signal frequency of 1000 Hz was used, to match field observations.

For the purposes of modelling, the in situ values were adopted for basalt and likely values selected for the ultramafic:

Basalt: $V_p = 6.7$ km/s; $V_s = 4$ km/s; $\Delta = 3$ gkc
Komatiite: $V_p = 5.5$ km/s; $V_s = 3.8$ km/s; $\Delta = 2.87$ gkc

This represents a most favourable situation, with P-wave reflection coefficient of 0.12. Furthermore, the modelling assumes a plane specular reflector of infinite extent, whereas the actual interface is likely to be irregular, reducing its effectiveness as a seismic reflector. However, the modelling certainly provides a good indication of the likely timing of events, given the accurate basalt velocity and the appropriate geometry. It also conveys the relative amplitudes of the various arrivals.

Figure 4 shows the computed seismograms. The two components represent motion parallel (Y) and perpendicular (X) to the geophone array. The direct P wave is dominant on the Y component; the direct S and Rayleigh wave on the X component. The amplitude of the shear/Rayleigh-wave is more than double the P-wave amplitude. Two separate reflections from the interface can be seen: a pure S reflection (SS), and a mode converted readily distinguished SP reflection. The PP reflection arrives at about the same time as the direct S/Rayleigh wave, and is obscured by it. The SP and SS reflection amplitudes are only 2% that of the direct S wave. For more realistic reflection coefficients, which are likely to be only one-third that assumed in the simulation, the detection and identification of the signal reflected from the contact would be extremely difficult, especially in the presence of noise (such as due to machinery, which can be quite high in a mine).

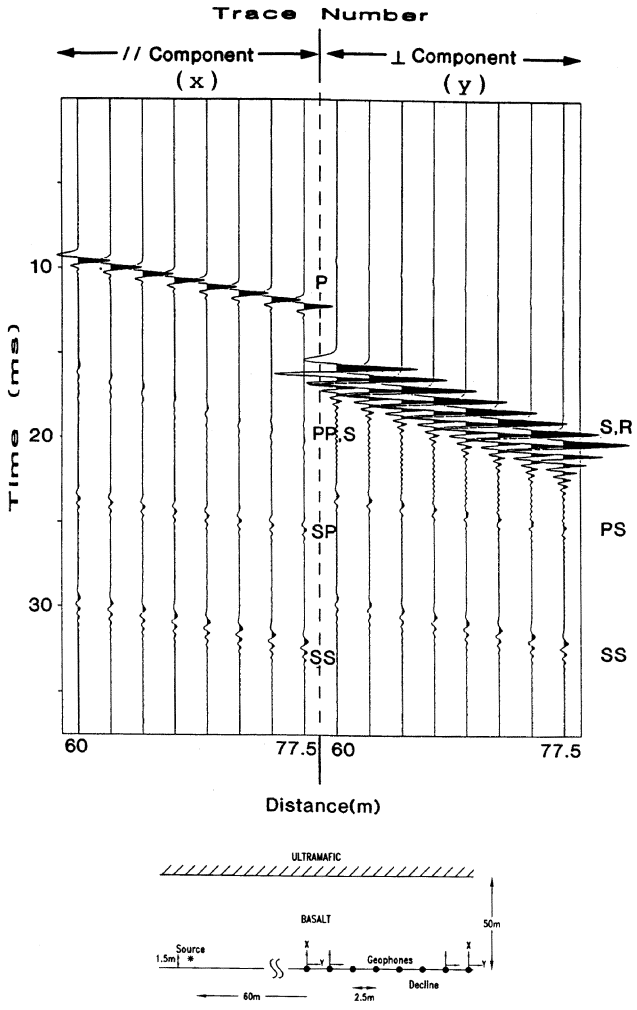

Figure 4: *Theoretical 2-component seismograms for a single reflector (basalt/ultramafic contact) 60 m from the tunnel wall containing source and receiver array. The PP reflection is obscured by the direct S and Rayleigh arrivals.*

CROSSHOLE/VSP SEISMIC FIELD SYSTEM

Seismic source

The most commonly used seismic sources for the mine development surveys conducted to date, and the crosshole/VSP experiments reported herein, are hammer blows and detonators. For early exploration-stage seismic surveying (e.g., surface reflection profiling) more energetic sources, such as 1 kg explosive charges in 5 m deep shotholes, are required to achieve the requisite range and depth.

Returning to the in-mine experiments, hammer impacts are achieved using a 10 lb sledge hammer which is struck against the wall of the mine tunnel. Various means of triggering have been tried, but the most successful seems to be a piezoelectric inertia switch mounted on the handle of the hammer. Careful attention needs to be paid to the consistency of the hammering, to ensure a repeatable source signal. In some environments the signal-to-noise ratio is not very good, making the use of the hammer source undesirable, even for distances of 50 m or less.

The electric detonator appears to be a most reliable source. It is a highly repeatable source and can be used in both underground (in-mine) and surface (crosswell) seismic surveys. The detonators are small enough to avoid damaging the boreholes in which they are fired but the holes must be water stemmed to prevent energy dissipation. One problem with using detonators down boreholes is that a new detonator has to be lowered downhole, sometimes several hundred meters, each time a new shot is required. This makes their use, in surveys involving sources in boreholes, very labor intensive and time consuming.

In general, explosive sources produce higher frequencies and larger amplitudes than hammer sources, making them more desirable in high-resolution imaging.

A new downhole electric discharge (sparker) seismic source, with the capacitors downhole, has been developed at Flinders University; it is described by Greenhalgh and Bierbaum (1997). The sparker system consists of a battery powered surface current source, connected via wireline winch cable to the downhole sparker probe (Figure 5). The probe itself is encased in 70 mm stainless steel tubing that is approximately 3 m long, weighing 22 kg. A digitally encoded manual winch makes accurate placement of the probe within a borehole. The accuracy is 2 mm in 10 m. The sparker is capable of rapid firing (every 15 seconds), the waveform is remarkably repeatable and each shot produces 500 Joules of energy. The signal from a single discharge is about equivalent to a detonator.

Receivers

For the various seismic experiments conducted over the past few years by the Flinders University group, two main types of receivers have been utilized, a hydrophone array and triaxial geophones.

Downhole hydrophone array

The hydrophone array, or borehole eel, used in these investigations was designed specifically for our requirements and was constructed by Australian Sonar Systems in Adelaide in 1993.

The primary factors considered in its design were that it had to fit into the narrow boreholes (≈ 46 mm) in the underground mine environment, it had to be rigid enough to be 'pushed' into the horizontal or declined holes and must be robust enough to stand a lot of wear and tear. Given the scale of the mine seismic problem the hydrophone elements had to be close together, of the order of one to two metres. Figure 6 shows the basic configuration of the array (acoustic module, support cable and end connectors) with details of the hydrophones and general assembly. It is a 24-channel array of 50 m aperture, connected to a 150 m long leader cable. At a diameter of 30 mm and base radius of 0.5 m, the eel is suitable for deployment in boreholes of 45 mm diameter to a depth of 200 m. The hydrophones have a frequency range of 50–2000 Hz and dynamic range of 80 dB.

The array is provided with a Front End Conditioner (FEC) which provides power to the array pre-amplifiers, buffers the array channel outputs and enables the level of the output to match the input of the recording device.

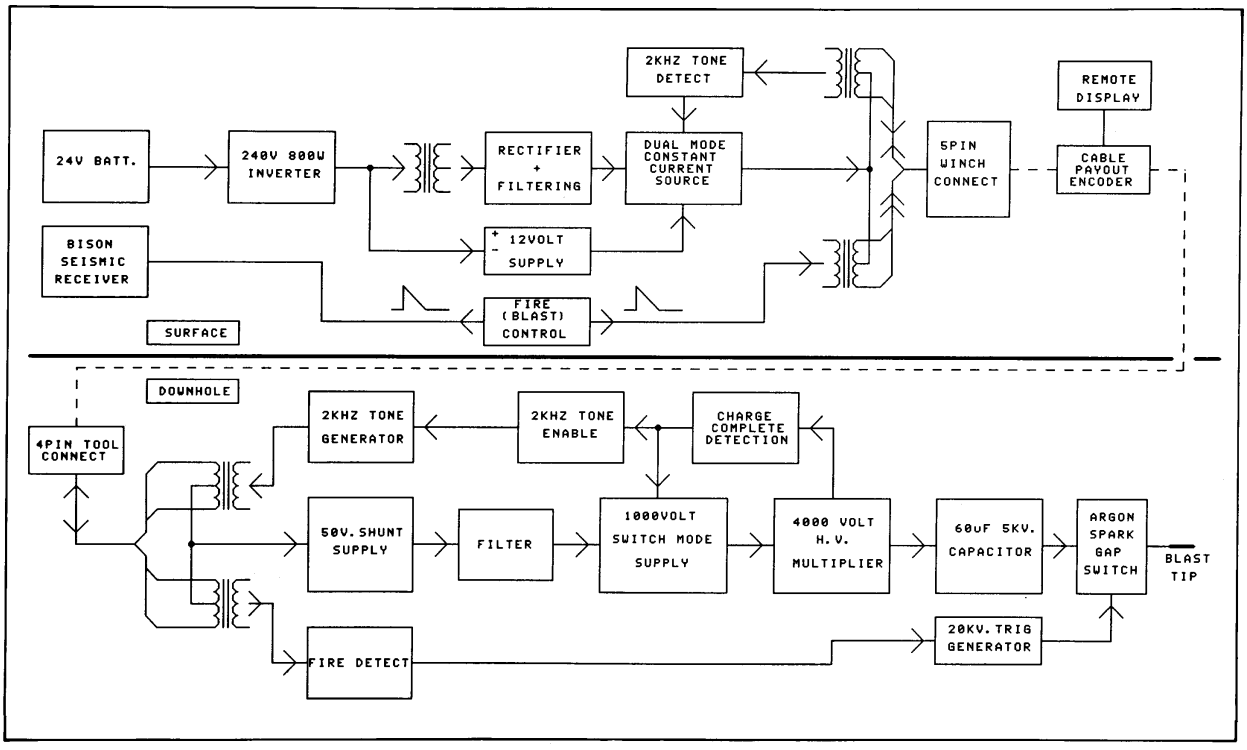

Figure 5: *Block diagram showing major components of the downhole sparker sound source.*

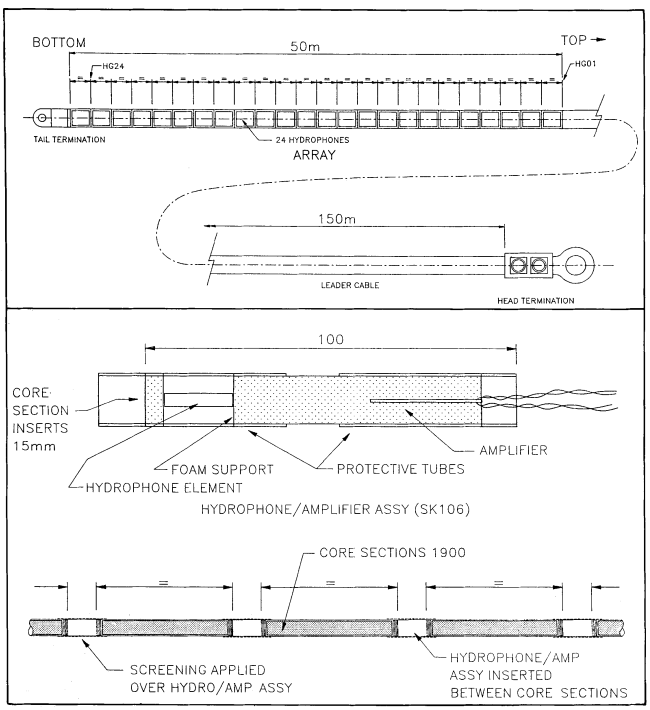

Figure 6: *Configuration of the downhole hydrophone array.*

The hydrophones are immersed in foam rubber with the wires wrapped and twisted on the outside. Each hydrophone has a sensitivity -200 dB re 1(Pa and is attached to a low noise preamplifier of high output impedance, with a gain of 45 dB. The array core is filled with a low density electrically inert fluid (isoparaffin) to give it neutral buoyancy.

The array/cable assembly is capable of withstanding a tensile load of 30 kN (3 tonnes applied axially and 1 tonne applied tangentially). The module is mounted on a winch drum of 500 mm radius and was therefore designed to withstand the stresses and strains of repeated bending around the drum while subject to a tensile load of 10 kN. The hydrophone is covered by a jacket made of a thermoplastic material which provides protection from abrasion during the deployment/retrieval operation in the borehole. The total power supply for the complete system can be provided by standard 12V batteries. Figure 7 shows the hydrophone array being deployed in a surface crosshole experiment.

Triaxial geophones

Triaxial geophones have been used for in-mine cross-gallery, reflection, and VSP investigations. These sensors, designed and built at Flinders University, utilize three 100 Hz Geospace GS 100 moving coil elements. These are high frequency geophones having 0.7 V/cm/s intrinsic voltage sensitivity. The three component sensors, placed in mutually perpendicular positions, are housed inside a 50 mm × 200 mm solid PVC tube. The detector is usually positioned with the longitudinal component along the borehole, the transverse component parallel to the gallery and

Figure 7: *Photograph of the eel on its drum after being lowered downhole.*

the vertical component along the hole. (Before processing the data the components are vector rotated into the 3-D mine coordinate system).

Each detector unit is fitted to a special anchor which is permanently grouted to the bottom of specially drilled holes in the tunnel wall. Although the anchor provides good detector-rock coupling it is still not free of the effects of cantilever resonance. Ideally, to reduce these resonance effects, the geophones should be sacrificed in the hole by surrounding the entire unit with grout and thus achieving rigid coupling. In view of the expense of manufacture of the geophones and the limited number available for each survey, the decision not to entomb the units was made at the risk of inferior performance.

Digital recording system

A 24-channel Bison 7024 digital instantaneous floating point signal stacking seismograph has been used as the recording device in all experiments. The detector outputs are sent to the seismograph via two twelve channel multi-core spread cables. The seismograph offers high dynamic range and a wide choice of input parameters such as record length, sample rate, filter settings, delay times etc. Record lengths are usually 100 ms with a sample rate of 0.1 ms. A built-in high resolution, high contrast thermal printer provides monitor records, if required, for each shot.

The seismograph is powered by a 12V lead-acid battery, which needs to be recharged on a daily basis. A second battery is used to power a Toshiba laptop computer which is connected to the seismograph via a RS-242 cable and used to observe each shot record. The digital data

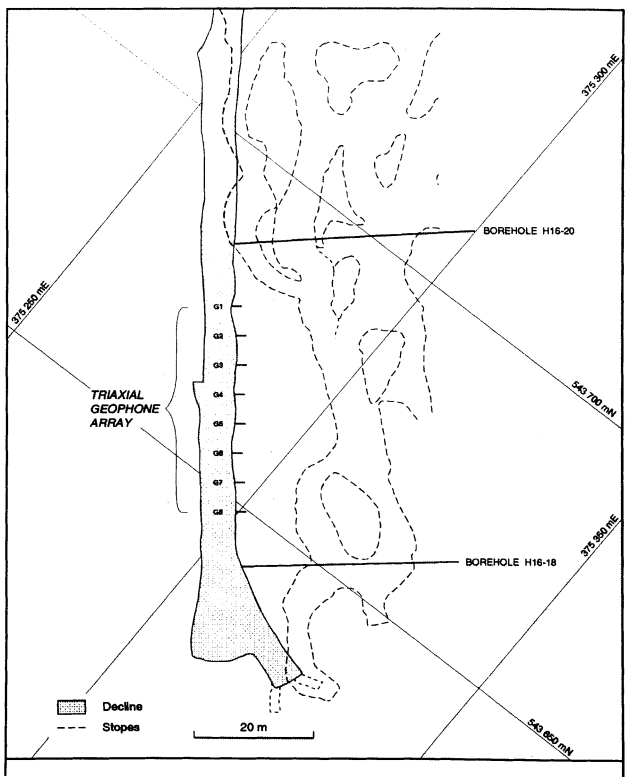

Figure 8: *Hunt mine seismic test site showing source-receiver boreholes, geophone array along decline, and stope geometry 20 m above decline.*

retained in the stacking memory of the Bison is downloaded to the computer, where each Bison file is converted to SEG-Y format. All files are backed up on floppy disc for storage and later processing.

UNDERGROUND SEISMIC IMAGING

A combined seismic tomography and reflection experiment was carried out at Hunt mine, 16 level, so as to assess the usefulness of underground seismic methods in mapping stope geometry and hard rock geological structure. A companion borehole radar experiment was carried out at the same site (Mason *et al.,* 1994) but only the seismic results will be presented here.

The test site

Figure 8 is a plan view of the test site. It shows the locations of the seismic boreholes DDH 16-18 and DDH 16-20 in relation to the D zone decline at the 16 level, and the overlying stopes. The stations G1, G2 …G8 are the collar positions of the triaxial geophones along the tunnel as well as being hammer impact points (see next section). The boreholes 16–18 and 16–20 were drilled downwards at an angle of 30° from the horizontal (so as to hold water), to a depth of 45 m. The distance between borehole collars is approximately 55 m. The volume of rock to be imaged was largely bounded by the decline, the two boreholes, and horizontal planes located 50 m above and below the level of the decline. The stopes of the BO5 ore surface are at a height of about 20 m above the borehole collars. This can be seen in Figure 9 which gives two geological cross-sections in the vertical planes of the boreholes. The additional pair of upward inclined boreholes shown, DDH 16-19 and DDH 16-08, were used for the radar experiment. Most of the ore in the vicinity of the seismic/radar test site has been mined out. The 16 level represents the deepest development of the mine. Extraction is continuing to the immediate south of the survey area. In fact, mining activity dictated that the geophysical work be undertaken on the afternoon and night shifts, when boggers were not operating in the decline.

Figure 9 gives two geological cross sections in the vertical planes of boreholes. The original ore shoot (pre-mined) is about 2 m thick and 20–30 m wide, and occupies the base of several troughs within the contact surface between the footwall basalt and the hanging wall ultramafics. There is remnant ore in the stopes where the surface has thickened in the form of local "jags". The ore has about a 2:1 density contrast with the enclosing rock, and possibly presents a slight velocity decrease (say, 5000 m/s vs 6000 m/s). The computed reflection coefficient for the idealised case of a plane, laterally continuous mineralised surface is about -0.11. In practice, the finite width of the ore, its discontinuous nature, and the roughness of the surface would greatly diminish its reflectivity, especially for wavelengths of comparable size to the structure. The ore would behave more as a diffuse diffractor than as a mirror. Furthermore, the target will only "reflect" sound back to the receiver array if illuminated from the right angle. The stope cavities themselves, rather than the small remnant mineralisation within them, are the more likely reflectors in this survey. The air/rock interface presents a perfect reflecting surface (reflection coefficient of -1), but once again the received signal will be downgraded by the finite extent (length and width) of the tunnels, and the finite wavelength. For a 1000 hz seismic signal, the wavelength is about 6 m (not unlike the radar wavelength), which is of the same order as the width of each stope.

The host medium is hardly homogeneous. Even within the footwall basalt there is considerable variability in composition and alteration, and hence elastic properties, as revealed by the two drill cores. There are several faults, fractures and quartz veins, as well as a porphyry sheet (see Figure 9), which disturb the host rock.

Seismic experiments

Three separate experiments: Crosshole survey, Hammer source VSP survey, and Explosive source inverted VSP, were conducted at the site shown in Figure 8.

Crosshole survey

The crosshole survey entailed shots in hole H16-20 at 1 m depth spacing, from 3.2 m to 42.3 m, and recording on a hydrophone array in hole H16-18, at 1 m spacing, over the depth range 0 m to 41 m. Since the

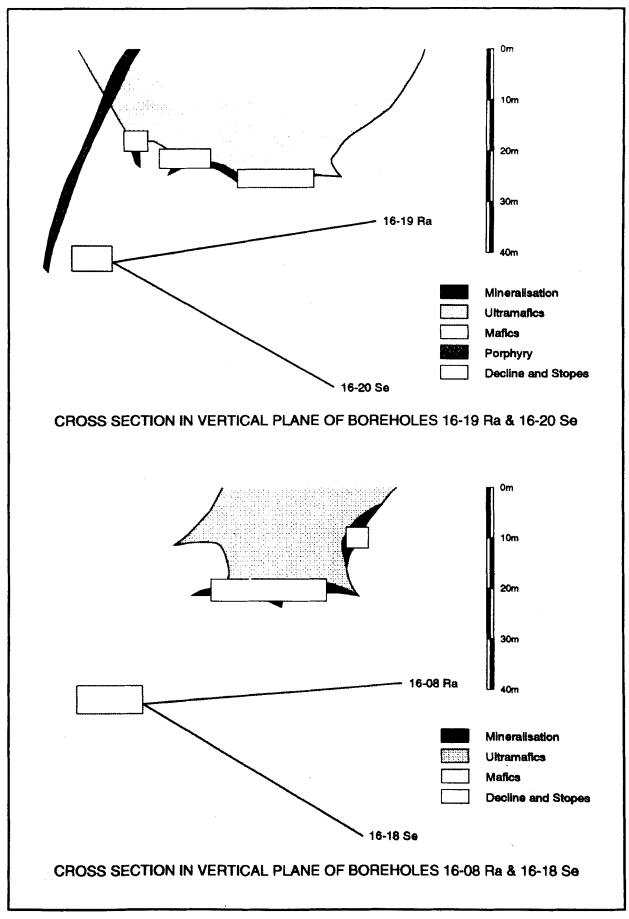

Figure 9: *Cross section at boreholes H16-18 and H16-20, showing simplified stope geometry and ore troughs.*

hydrophone array has its detectors at 2 m intervals, and is limited to just 24 channels, the 1 m receiver array was synthesised by shooting twice at each depth level in hole H16-20, once for hydrophones at positions 0 m, 2 m, … 40 m, and again after displacing the eel by 1 m in the hole such that the elements were as positions 1 m, 3 m, … 41 m. It was not possible to push the hydrophone streamer into the hole any deeper than 43 m. The first hydrophone element lies one metre from the end of the eel. The length of the active section is 46 m (for 24 elements = 23 × 2 m), and so the top two elements of the streamer were actually out of the hole in the decline on each deployment. These two channels (1 and 2) were ignored, along with channel 24 (base of the eel), which had been damaged by salt water incursion into the preamplifier on a previous deployment. Thus the number of useable recording channels was reduced from 24 to 21 on each shot. The total number of seismic records collected in the crosswell experiment was 40 × 2 × 21 = 1680.

It would have been desirable to have collected the seismic data at a closer spacing (shot and receiver interval of 0.5 m or less), but this would have greatly increased the acquisition time. We were limited largely by the time to load and place each shot.

Hammer VSP experiment

The hammer VSP experiment was the first phase of the work undertaken. It involved placing the hydrophone array in hole H16-18, with detectors at 2 m intervals over the depth range 1 m to 41 m, and impacting the tunnel wall with a 10 lb sledge hammer along the decline, at one-quarter station positions, from G1 to G8.5 (1.25 m intervals). This is a multilevel, walkaway VSP recording geometry. The number of seismograms collected was 31 × 21 = 651.

Triaxial VSP experiment

This experiment was a reversed multilevel walkaway inverted VSP. It entailed having shots at 1 m spacing in both holes H16-18 (depth range 3.2 m to 42.3 m) and H16-20 (depth range 3.6 m to 42.6 m) and recording on eight three-component geophones along the decline wall, (G1 to G8 — see Figure 8) at a nominal spacing of 5 m. The sensors were placed in 2 m deep horizontal holes drilled perpendicular to the tunnel axis, oriented into position, and then grouted permanently into each hole. The orientation system was such that the X component was parallel to the decline, with its positive terminal pointing northwest (up the decline), the Y component pointing along and into the axis of the hole (northeast), and the Z component vertically downwards. The purpose of using 3-component receivers was to achieve directional sensitivity in the response, which is of potential benefit in 3-D imaging with a limited number of sensors arranged in a fairly short linear array.

The number of records acquired in the triaxial VSP experiment was 40 × 2 × 8 × 3 = 1920.

SIGNAL CHARACTERISTICS AND NOISE

Figure 10 is a sample set of shot gather records from the crosshole experiment. Each panel represents a separate shot (depth 22.2 m, 23.2 m, etc.) recorded on 21 hydrophone receivers at depths of 1 m, 3 m, … 41 m. The first arrival is the direct P wave. The record is full of other events which seem to move out in both directions with the approximate speed of sound in water. This is best seen on receiver gathers (Figure 11), which reveal the origin of these events as the top, bottom and middle of the shothole. These secondary events are tube wave to P and S conversions

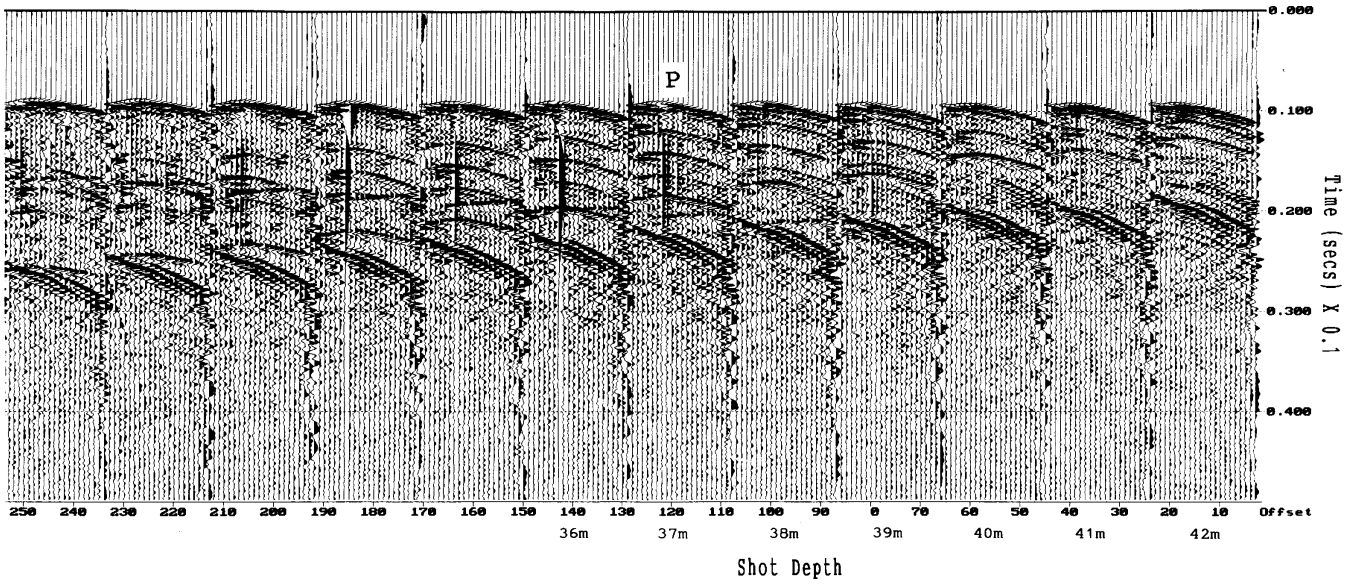

Figure 10: *Set of shot gather crosswell hydrophone records for shots in hole H16-20 and receivers in hole H16-18. Shot depth spacing is 1 m, receiver spacing is 2 m.*

at each end of the hole, and also from an impedance boundary (fracture zone) midway along the hole. The top and bottom of the hole present barriers to the shock front set up from the actual source in the hole. They behave as secondary "sources" of body waves, which then radiate out into the medium and are recorded on the receiver array, superimposed on the direct and reflected arrivals from the actual shot.

There is a family of tube waves in the shothole (velocities 1.2 km/s to 1.5 km/s), each of which undergoes mode conversion. The body waves (from true and secondary sources) can then excite tube wave arrivals in the receiver hole from both ends as well as from any fractures or other discontinuities in the hole. This makes for a very cluttered record and represents a severe form of coherent noise contamination. It is difficult to remove. Velocity filtering is partially effective (due to low water wave velocity in the receiver gather domain) but it can only be done if the waves are not velocity aliased, which means a very close shot spacing (say, 0.25 m). Unfortunately this was not the case with the Hunt experiment. The tube wave problem arises largely from shooting in a water-filled hole. Explosions in dry holes don't generate tube waves, but they don't generate much body wave energy either, because of the very poor coupling.

The detonator source produced high amplitude, high frequency (up to 3000 Hz) signals. The high frequencies are important for getting reflections from small objects like ore shoots, and for having the requisite resolution.

The 1 m shot and receiver interval used on the crosshole survey, the 5 m geophone spacing used on the triaxial VSP, and the 2 m hydrophone interval/1.25 m impact interval used on the Hammer VSP, were inadequate to combat the low velocity coherent noise, which became aliased at the high (KHz) frequencies involved.

The seismic work at Hunt was conducted mainly at night. Background noise was plentiful, and included vibrations from ventilation fans, pumps, surface drilling above, inductive pickup, and boggers operating nearby. On some occasions the noise was so high that the recording had to be discontinued. Apart from the noise, the seismic survey was interrupted by several instrument malfunctions.

TOMOGRAPHIC IMAGING

Procedure

Tomography is a two-dimensional image reconstruction procedure. The image plane in the present context was formed by the two dipping boreholes and the section of decline joining the two hole collars. These three observation lines are not actually straight nor perfectly co-planar, because of the slight irregularity of the tunnel and the drillholes. But as a starting point for tomographic inversion, we computed the best-fit plane to the three lines and projected the actual shot-receiver positions onto this plane.

The input data comprised the first arrival times (after static correction) for the crosshole and the hammer VSP records. That is, only the hydrophone data were used in the reconstruction. Over 2300 raypaths criss-cross the image plane to yield good angular and spatial coverage. The source and receiver positions along the three arrays used to form the "U" geometry are at roughly 1 m spacing. The medium was divided up into cells of dimension 0.25 m × 0.25 m.

The tomography procedure begins with a uniform (average) velocity model and then iterates through using a multistage, sub-space method (Cao and Greenhalgh, 1995) in which the long spatial wavelength velocity variations are solved for first, progressively adding in the short wavelength features. A conjugate gradient type algorithm is at the heart of the model update procedure, details of which are given by Zhou, Greenhalgh and Sinadinovski (1993).

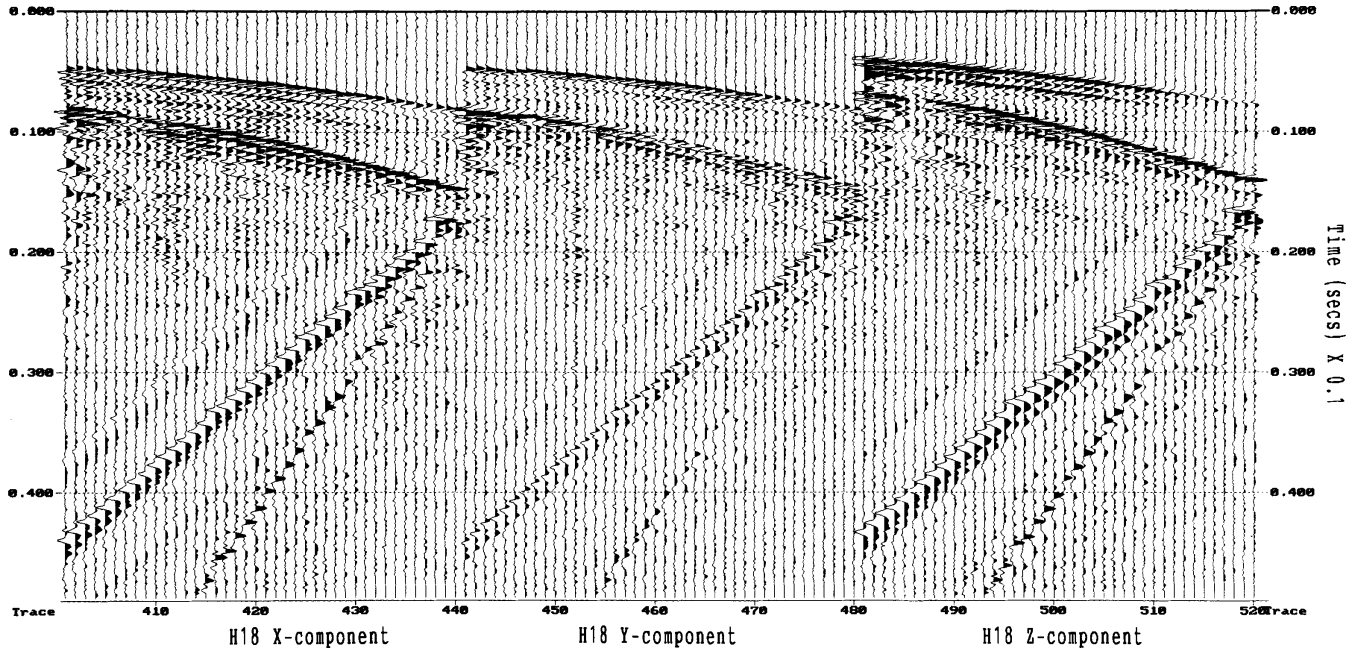

Figure 11: *Set of receiver gathers for crosswell experiment, showing direct P and S waves plus tube wave generated events at top, bottom and middle of shothole. Trace spacing is 1 m.*

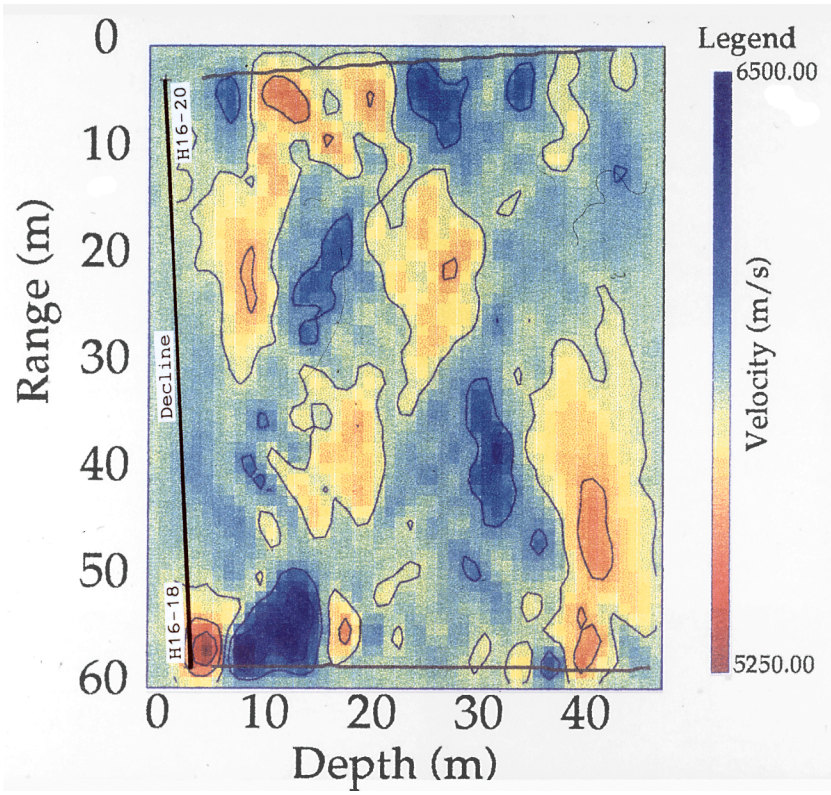

Figure 12: *Tomographic reconstruction of the first arrival VSP and crosshole data at Hunt mine.*

Tomogram features

Figure 12 shows the final tomogram obtained. The colour code at the side of the map defines the various velocity values. The boreholes have been superimposed on the tomogram to give the proper perspective. (The crosses '+' denote collar positions in the decline).

The velocities vary from about 5300 m/s to 6400 m/s. From the geological log of the holes we know that the rock type is entirely basalt, but the velocity field is anything but homogeneous. The inhomogeneity is presumably due to changes in alteration and geochemistry of the basalt. The presence of quartz veins and fractures will also affect the measured velocity values.

Ultrasonic velocity measurements were carried out on eight core samples taken from the two holes, to aid tomogram interpretation. The samples included the major change in basalt type and condition. Velocity results are given in Table 3. The massive basalt gives high velocity of 5900 m/s. That having abundant disseminated magnetite yields lower velocity, as expected, through the effect of increased density. The ankerite-albite altered basalt gives much lower velocity, of just 2700 m/s. The massive quartz vein gives a velocity of 4700 m/s, similar to that of the amphibole rich basalt. These velocities are all lower than those obtained in situ from the seismic tomography experiment. This can be largely explained by the fact that the rock in situ is under considerable lithostatic pressure. It is well known that pressure increases velocity due to the closing of fractures and reduction of porosity.

Table 3: ***Ultrasonic velocities of core samples from Hunt H16-18.***

Sample No.	Rock Description	Longitudinal Velocity (m/s)
1	Amphibolite rich basalt	4640
2	Massive basalt	5930
3	Massive basalt with abundant disseminated magnetite	3990
4	Massive quartz vein	4690
5	Awaiting XRD results	5710
6	Epidote altered basalt	6130
7	Biotite-rich basalt and disseminate pyrite	5240
8	Alteration zone: ankerite–albite altered basalt	2680

If the relative velocity variations, rather than the absolute variation are considered along borehole H16-18, then the tomogram velocity variation is well matched by the ultrasonic velocities. The high, medium and low velocity zones in the tomogram seem to correlate well with the mineralogy and alteration of the basalt. This is an encouraging result, especially given the fact that only single sample determinations for each rock "type" were made. Apart from random errors on single samples, which can be smoothed out by multiple sample measurements, it should also be remembered that the laboratory sample may not be representative of the rock behaviour in situ, because of the absence of macrofeatures such as fractures. Alternatively, macrofeatures such as 1 m wide quartz veins may have little effect on 6 m long seismic wavelengths in the field, but multiple mm wide fractures in a laboratory sample may dramatically affect the velocity obtained using a 1 cm long ultrasonic wave.

It thus appears that seismic tomography at this location offers a useful lithologic mapping tool. It is unfortunate that no mineralisation lies within the image plane. The boreholes dip downwards, whereas the ore is in the stopes above the decline.

THREE-DIMENSIONAL REFLECTOR IMAGING

The principal targets of the crosswell/VSP reflection experiment were the stope tunnels and residual ore, lying about 20 m above the decline, as explained earlier (see Figure 9).

The reflection imaging procedure is described by Sinadinovski *et al.* (1995). In simple terms, it is a pre-stack Huygens-Kirchoff migration method.

The procedure involves breaking up the volume into small cells and calculating the probability that a diffractor/reflector exists at each grid point, by summing amplitudes over all shots and geophones. The ray-paths are first traced in 3-D from every shot to every voxel, and back to every receiver. The corresponding traveltimes (for the assumed wave type: PP, PS, SP, SS) define the search trajectory through the traces. For three-component receiver data, the azimuth and inclination of each computed ray permit the additional projection of the signal vector into the plane of the wavefront (S) or parallel to the ray (P). Constructive interference will occur only for those voxels at which seismic scattering take place.

We modified the procedure for the Hunt experiment in two ways. First, we used a semblance-based measure of trace energy alignment, by forming all of the possible cross products of sample amplitude over a 10 to 20 point sliding time window for each gather. Secondly, we performed a partially coherent migration by adding only the absolute values for each shot gather, which were coherently summed individually, over time, receiver position, and component. The reason for doing a partially rather than a fully coherent migration is to minimise the effect of shot static-type timing errors and other random fluctuations.

The cell size used in the volume interrogation procedure was a 1 m cube. The grid size was $60 \times 60 \times 15$, or 54 000 voxels. Larger cells were also explored, but computer memory limitations precluded an increased 3-D grid.

The data to be migrated must undergo some pre-treatment, such as 3-component rotation, muting of direct P and S wave arrivals (10 to 20 sample suppression window) and gain function application to boost the later arrivals. The input data comprise the velocity field, the source

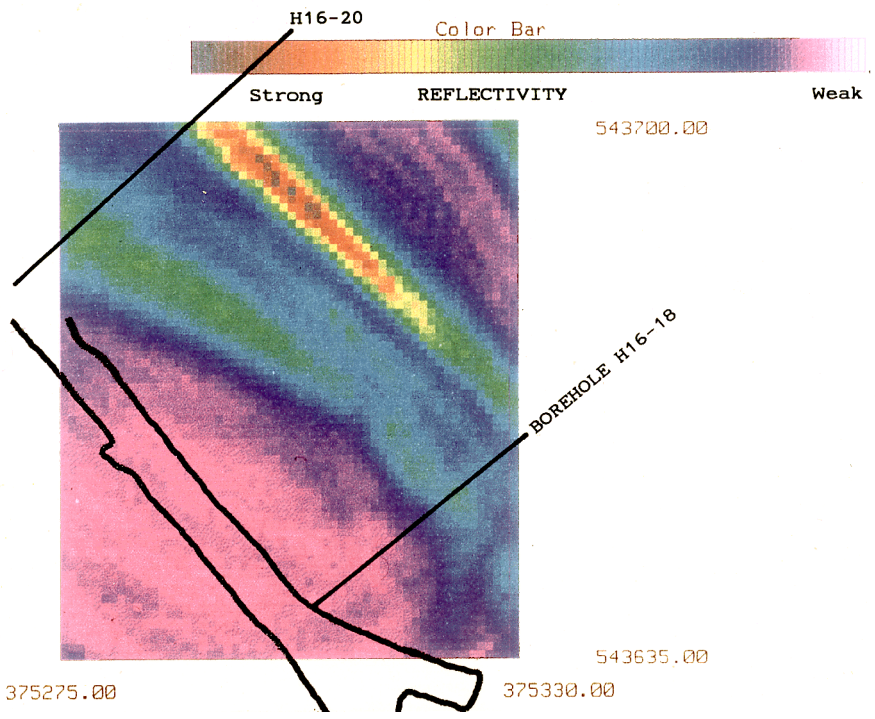

Figure 13: *P-wave migration result for VSP/crosshole data. The map is a horizontal slice of the 3-D volume at the -234 m level. The scatterers parallel the stope geometry.*

receiver coordinates, and the field seismograms. The process is repeated for the various modes (PP, SS, etc.), if desired.

The output from the migration is a set of positive numbers at each point in the 3-D grid, which represent the scatterer probabilities. These numbers are colour coded according to some appropriate non-linear sale (e.g., logarithms) and the image planes (horizontal slices through the volume) then displayed at various depths.

Results

The data subsets used for the migration were the statically corrected and pre-processed records from:

- the triaxial VSP experiment: 80 shots, 8 receivers, and
- Crosswell experiment: 40 shots, 2×21 receivers.

The individual data sets were migrated separately, as well as being combined into a single migration. The attraction of a combined geometry is that the reflectors are illuminated from a greater range of angles.

Figure 13 is a horizontal slice through the final P-wave migration 3-D volume at the -234 m elevation level. This elevation corresponds to the approximate average position of the stope floor across the survey area. The southwest stope tunnel actually drops a depth of about 4 m over a horizontal distance of 55 m between the two boreholes, from an elevation of -231 at the northern end to an elevation of -235 m in the south. The northeastern stope floor maintains an elevation of -234 m over its northern extent.

The warm colours (brown, red, yellow) in Figure 13 indicate the strongest scatterer positions, whereas the cold colours (blue, purple) indicate the absence of any reflectors. Geographical coordinates, as well as the projected position of the D zone decline (20 m below the elevation shown), are given on the map to aid location/identification of features. The migration results show a striking correlation with the known mine workings (see Figure 8). The two green coloured elongate zones of moderate reflectivity, which sub-parallel the decline, delineate the stopes. The southwestern ridge bends in close to the decline at its northern end, following the actual stope cavity. The region of strong reflectivity, coloured red, seems to coincide with the far boundary of the northeastern tunnel. The reflectivity may well be enhanced by the curvature of the ore trough and the sharp lip of the structure, as seen in Figure 9. This would cause a focussing of back-scattered energy, as observed my Mason *et al.* (1992) in the decline radar profile. The presence of residual, unmined ore on this side of the stope (see Figure 9) may also be contributing to the strong reflection signal.

It is interesting to observe on the computer how the reflection (migration) pattern changes with elevation. Migration slices at the -230 m and the -240 m levels (not shown), which are just above and below the stope floor and roof elevations, respectively, yield reduced reflectivity from the maximum which occurs within the -237 m to -236 m depth range.

The finite time window used in forming the semblance, as well as the finite wave length of the signal (say, 6 m) means that resolution is limited, and features get averaged, or smoothed in the migration, over a spatial distance of at least several metres. Migration images obtained at elevations of -226 m and -246 m (not shown), exhibit almost no structure, confirming that the reflectors are confined in depth to the vicinity of the stopes.

CONCLUSIONS

A high resolution seismic hardware-software system has been developed for cross-hole/VSP imaging of ore bodies and associated hardrock geological structure, either within mines or from the Earth's surface using available boreholes.

A body of laboratory data on the elastic properties of nickel sulphides and host rocks has been acquired as an aid to interpretation.

Although the seismic signals are of high frequency and high quality, records are strongly contaminated by tube wave and mode conversion noise. Dense arrays of sources and/or receivers are needed to enable proper pre-processing of the data prior to imaging.

An example of an underground survey at the Hunt mine, Kambalda, demonstrates the possibility of both tomographic imaging, to map velocity inhomogeneities, and reflection imaging to delineate stope geometry. The seismic maps show a striking correlation with the known geology.

The seismic images (especially reflection) are difficult to obtain and not easy to relate to mineralisation. Companion electrical images such as radar, RIM and applied potential, are needed to aid interpretation and are likely to see increased use in mine development over the next few years. The seismic method offers great promise in prospect exploration. We are working on improvements to borehole geophysical instrumentation and at developing more versatile image reconstruction procedures.

ACKNOWLEDGEMENTS

We wish to acknowledge the support and cooperation of Peter Williams and Greg Turner from Western Mining Corp. in the conduct of this work.

REFERENCES

Adam, E., Milkereit, B., Arnold, G., and Pineault., 1996, Seismic response of the Bell Allard orebody, Matogami Québec: 66th Annual SEG Meeting, Denver, Colorado, Nov. 10-13, Abstracts 634-637.

Campbell, G., and Crotty, J.H., 1988, The application of 3-D seismic surveys to mine planning: South African Chamber of Mines MINTEK Seminar, 4th March, 1988.

Cao, S., and Greenhalgh, S.A., 1992, Finite-difference simulation of P-SV wave propagation: a displacement potential approach: Geophys. J. Int. **109**, 525-535.

Cao, S., and Greenhalgh, S.A., 1995, Relative-error based non-linear inversion: application to seismic travel time tomography: Geophys. J. Int. **121,** 684-694.

Carneico, D., and Gendzwill, D., 1996, High-resolution seismic reflection survey in a deep gold mine: 66th Annual SEG Meeting, Denver, Colorado, Nov. 10-13, Abstracts 2069-2071.

Cosma, C., 1983, Determination of rock mass quality by a crosshole seismic method: Bull. Intl. Assoc. Eng. Geol., 26-27.

Cowden and Roberts, 1990, Komatiite hosted nickel sulphide deposits Kambalda: *In* Geol. and Min. Dep. of Aust. and PNG, Hughes, F.E., ed., Aust. Inst. Min. Met., Melbourne, 567-581.

Dahle, A., Gjoystdal, H., Grammeltvedt, G., and Soyland Hansen, T., 1985, Applications of seismic reflection methods for ore prospecting in crystalline rock: First Break, 3, 9-16.

Duncan, G., Downey, M., Leung, L., and Harman, P., 1989, The development of crosshole seismic techniques and case studies: Exploration Geophysics **20** (1/2), 127-130.

Friedel, M.J., Jackson, M.J., Scott, D.E., Williams, T.J., and Olson, M.S. 1995, 3-D tomographic imaging of anomalous conditions in a deep silver mine: J. Applied Geophysics **34**, 1-22.

Fullagar, P., Mason, I.M., and Greenhalgh, S.A. 1992, High resolution geophysical imaging for exploration and development of nickel sulphide orebodies: Western Mining Corp., Report K/3470.

Galperin, E.I., 1984, The Polarisation Method of Seismic Exploration: D. Reidel Publishing Co., Boston.

Gendzwill, D.J., and Brehm, R. 1993, High resolution seismic reflections in a potash mine: Geophysics **58**, 741-748.

Greenhalgh, S.A., and Bierbaum, S., 1997, A downhole sparker sound source for mineral seismic applications: Submitted for publication.

Gustavsson, M., Moren, P., Pihl, R., and Ivansson, S., 1984, An experiment with the seismic cross-hole method in an iron mine: The Leading Edge 3: **11**, 143-145.

Harman, P., Leung, L., and Downey, M., 1987, Cross-hole seismic survey for mineral exploration in the West Kimberley Area, Western Australia: Exploration Geophysics **18**, 80-83.

Mutyorata, J.J., 1987, High resolution seismic reflection an exploration tool in an underground environment—example from Zimbabwe: Jour. African Earth Sci. **6(1)**, 109-115.

Nelson, R.G., 1984, Seismic reflection and mineral prospecting: Expl. Geophys. **15**, 229-250.

Peterson, J.E., Paullson,, and McEvilly, T.V., 1985, Applications of algebraic reconstruction techniques to crosshole seismic data: Geophysics **50**, 1556-1580.

Price, T.O., 1974, Accoustical holography as a tool for geological prediction: *In* Subsurface Exploration for Underground Excavation and Heavy Construction, Am. Soc. Civil. Engrs.

Reid, A.B., Polome, L.G., and Greene, B.W., 1979, Ultra-high resolution reflection in chromite detection: Presented at the 49th Ann. Int'l. Mtg. Soc. Expl. Geophys. New Orleans.

Ruskey, F., 1981, High-resolution seismic methods for hard rock mining: *In* Premining investigations for hardrock mines: Proc. U.S. Bureau of Mines Technology Transfer, Seminar Denver, 4-28.

Schmidt, G., 1959, Results of underground seismic reflection investigations in the siderite district of the Siegerland: Geophys. Prosp. **7**, 287-290.

Sinadinovski, C., Greenhalgh, S.A., and Mason, I.N., 1995, Three-dimensional reflector imaging of in-mine high frequency crosshole seismic data: Expl. Geophysics **26**, 325-330.

Singh, S., 1983, A study of shallow reflection seismics for placer-tin reserve evaluation and mining: Geoexploration **21**, 105-135.

Spencer, C., Thurlow, G., Wright, J., White, D., Caroll, P., Milkereit, B., and Reed, C., 1993, A vibroseis reflection seismic survey at the Buchans mine in central Newfoundland: Geophysics **58**, 154-166.

Wachsmuth, C.,, and Schmidt, E., 1962, Experience with the reflection seismograph in a mine within a slat plug: Geophys. Prosp. **10**, 491-496.

Wong, J., Hurley P., and West, G.F., 1984, Crosshole audio-frequency seismology in granitic rocks using piezoelectric transducers as sources and detectors: Geoexplor. **22**, 261-280.

Wright, C., Wright, J.A., and Hall, J., 1994, Seismic reflection techniques for base metal exploration in eastern Canada: examples from Buchans, Newfoundland: J.Applied Geophysics **32**, 105-116.

Young, R.P., Hutchins, D.A., McGaughey, J., Towers, J., Jansen, D., and Bostock, M., 1989, Geotomographic imaging in the study of mine induced seismicity: Pure and Applied Geophysics **129**, Nos 2/3, 571-596.

Zhou, B., Greenhalgh, S.A., and Sinadinovski, C. 1992, Iterative inverse techniques for DMNLS in seismic tomography: *In* Geotomography—Vol II, Society of Expl. Geophys. Japan, p.111-128.